USA) was used to determine the amount of cellular $PI(4,5)P_2$ according to the manufacturer's instructions.

Results

$PI(4,5)P_2$ accumulates at invadopodia formed in invasive human breast cancer cells. Localization of $PI(4,5)P_2$ in invadopodia was first determined by immunocytochemistry. MDA-MB-231 is a highly invasive human breast cancer cell line with a basal-like phenotype, the most aggressive form of breast cancers.[27] MDA-MB-231 cells were plated onto fluorescence-labeled gelatin and then stained with an anti-$PI(4,5)P_2$ antibody, whose specificity was validated previously.[24] MDA-MB-231 cells have been shown to form invadopodia, which are observed as dot-like accumulations of actin filaments (F-actin) associated with black areas formed by the degradation of fluorescent gelatin matrix. The $PI(4,5)P_2$ signals were mainly observed at the plasma membrane (Fig. 1, left). On the ventral surface of the
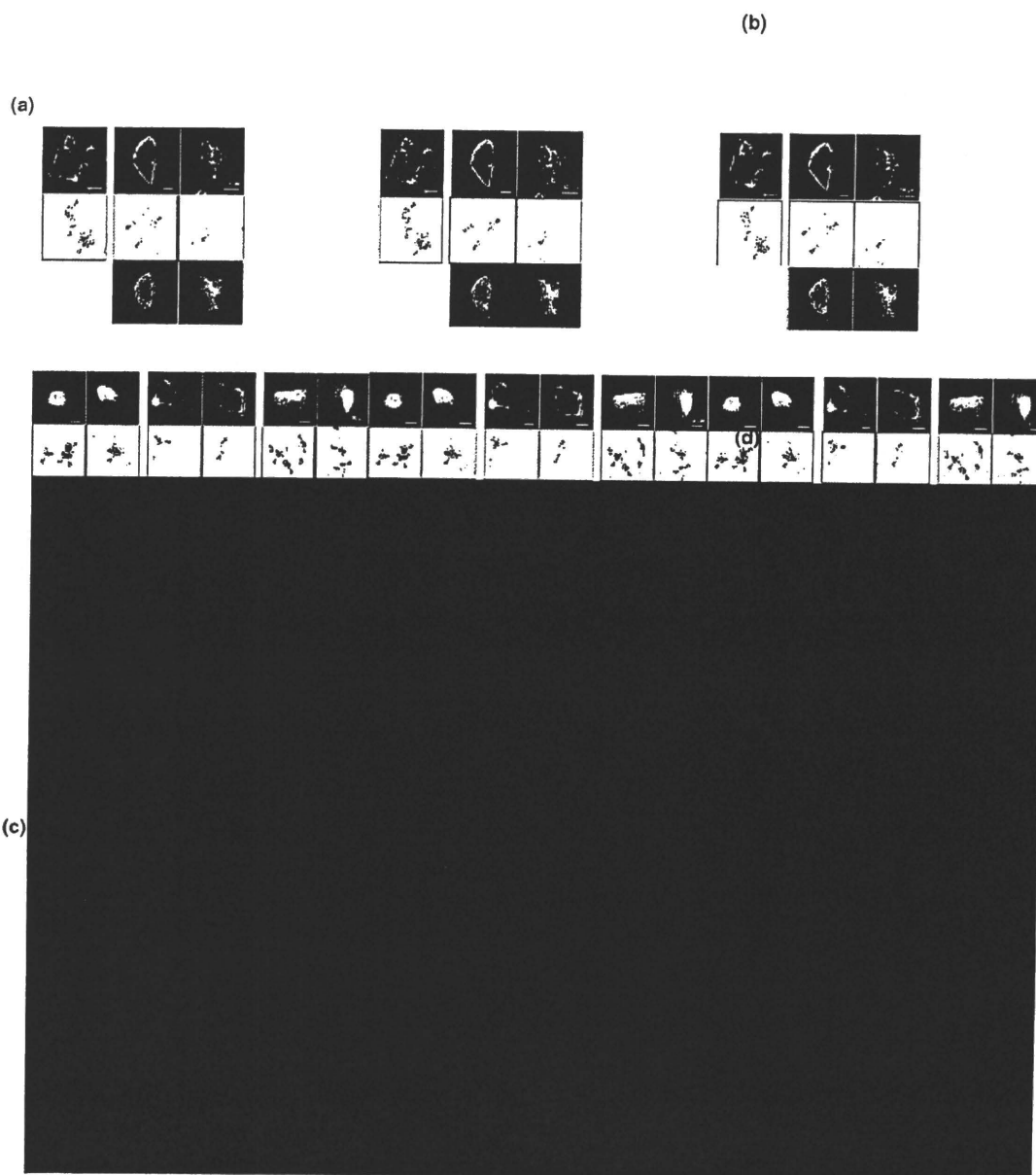
(a)

(b)

(c)

(d)

Fig. 2. $PI(4,5)P_2$ is necessary for invadopodia formation. (a) MDA-MB-231 cells were plated onto fluorescent gelatin-coated coverslips for 2 h and microinjected with mouse anti-$PI(4,5)P_2$ antibody. Cells were further cultured for 3 h to allow them to form invadopodia and then stained with phalloidin and antimouse IgG secondary antibody to detect injected cells. The arrowhead denotes the gelatin degradation sites. (b) Quantification of invadopodia activity. The degradation area of the gelatin matrix was calculated as described in the Materials and Methods and shown as a percentage of uninjected cells. Data are mean ± SEM (n = 95, 47, and 100 cells for uninjected, control (Ctrl) IgG, and anti-$PI(4,5)P_2$ antibody injected cells, respectively). *P < 0.04, Student's t-test. (c) MDA-MB-231 cells transfected with GFP or GFP-PLCδ1-PH constructs (WT and R40D) were cultured on fluorescent gelatin-coated coverslips. Representative microscopy images of the cells are shown. The arrowhead denotes the gelatin degradation sites. (d) The degradation area of the gelatin was quantified among cells transfected with the indicated constructs. Data are mean ± SEM (n = 51, 51, and 48 cells for control, WT, and R40D, respectively). **P < 0.02, Student's t-test.

cells, the PI(4,5)P$_2$ signals were observed as small vesicles and some of them were localized in close proximity to the degradation sites of gelatin formed by invadopodia (Fig. 1, right). The vesicular signals often surrounded the F-actin structures of invadopodia (Fig. 1, right). These observations indicate that PI(4,5)P$_2$ accumulates at invadopodia and associated gelatin degradation sites.

PI(4,5)P$_2$ is required for invadopodia formation. The role of PI(4,5)P$_2$ in invadopodia formation was then examined. Microinjection of an anti-PI(4,5)P$_2$ antibody was previously shown to inhibit the cellular functions of PI(4,5)P$_2$.[24] MDA-MB-231 cells were plated onto fluorescent gelatin and microinjected with control IgG or anti-PI(4,5)P$_2$ antibody. The cells were further cultured to allow them to form invadopodia and degrade the gelatin matrix. Cells injected with anti-PI(4,5)P$_2$ antibody showed a decreased ability to form invadopodia and degrade the gelatin matrix compared to the uninjected and control IgG-injected cells (Fig. 2a,b). It was also observed that microinjection of anti-PI(4,5)P$_2$ antibody tend to increase cortical F-actin (Fig. 2a). However, some of the cells injected with anti-PI(4,5)P$_2$ antibody showed impaired invadopodia formation without such changes in the actin cytoskeleton, excluding the possibility that the loss of invadopodia is secondarily caused by aberrant accumulation of F-actin. The role of PI(4,5)P$_2$ in invadopodia formation was also determined using a PLCδ1-PH domain fused to GFP (GFP-PLCδ1-PH). GFP-PLCδ1-PH specifically binds to PI(4,5)P$_2$ and therefore sequesters PI(4,5)P$_2$ upon overexpression.[28] Compared to control GFP-transfected cells, invadopodia formation and gelatin degradation were significantly impaired in cells overexpressing GFP-PLCδ1-PH (Fig. 2c,d). This effect was not observed when cells were transfected with the R40D mutant of GFP-PLCδ1-PH, which possesses a point mutation in an amino acid essential for PI(4,5)P$_2$ binding[29] (Fig. 2c,d). Although the GFP-PLCδ1-PH signals were almost exclusively observed at the plasma membrane, signals in the R40D mutant were mainly detected in the cytosol and the nucleus similar to the control GFP signals (Fig. 2c). These results demonstrate that PI(4,5)P$_2$ function is necessary for invadopodia formation and ECM degradation.

PIP5KIα is an essential regulator of invadopodia formation. PI(4,5)P$_2$ in mammalian cells is mainly produced by the PIP5KI family, which consists of three isoforms, PIP5KIα, Iβ, and Iγ. We next determined whether the PIP5KI family is involved in invadopodia formation. The expression of the PIP5KI family in MDA-MB-231 cells was examined by real-time quantitative PCR analysis. PIP5KIα was abundantly expressed in these cells, while the expression level of PIP5KIγ was only about 7% of that of Iα (Fig. 3a). The expression of Iβ was undetectable in this analysis (Fig. 3a), although the primer set used could efficiently detect Iβ expression when human cDNA mixture was used as a template (data not shown). These data indicated that PIP5KIα is the most abundantly expressed isoform in MDA-MB-231 cells.

In order to examine the roles of PIP5KIα and Iγ in invadopodia formation, cells were transfected with siRNAs targeting these enzymes. Efficient knockdown of each isoform was confirmed by RT-PCR analysis (Fig. 3b, left), and immunoblotting in the case of PIP5KIα (Fig. 3b, right). Cells with a reduced level of PIP5KIα showed a marked decrease in invadopodia formation and gelatin degradation activity (Fig. 3c,d). Similar results were obtained with another siRNA targeting a different region of the *PIP5KIα* gene (Fig. 3b,d). In contrast, such effects were not observed in cells transfected with PIP5KIγ siRNA (Fig. 3c,d), which should target both Iγ635 and Iγ661. Additionally, PIP5KIβ siRNA also had no effect on invadopodia formation (data not shown). These results indicate that PIP5KIα, among the PIP5KI family members, is specifically involved in invadopodia formation.

PIP5KIα knockdown does not affect PI3K signaling. PI3K activities are necessary for invadopodia formation in human melanoma cells.[30] Because PI(4,5)P$_2$ serves as a substrate of PI3K for generating PI(3,4,5)P$_3$, it is possible that suppression of invadopodia formation by PIP5KIα knockdown is due to the inhibition of PI3K signaling. To test this possibility, the effects of PIP5KIα knockdown on the activation of PI3K signaling were examined. EGF stimulation is known to activate PI3K signaling, which results in the phosphorylation and activation of the downstream target Akt. As expected, EGF stimulation markedly increased the amount of phospho-Akt in control cells
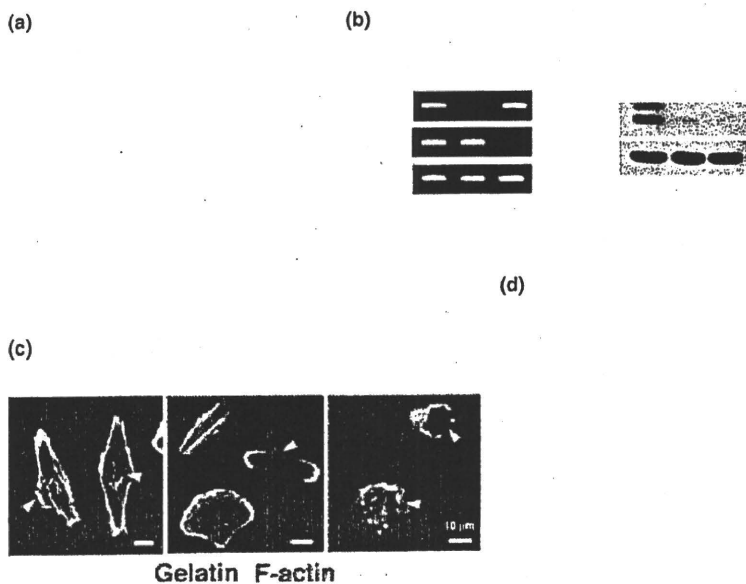
(a)

(b)

(d)

(c)

Gelatin F-actin

Fig. 3. PIP5KIα is an essential regulator of invadopodia formation. (a) Expression of PIP5KIs in MDA-MB-231 cells was analyzed by real-time quantitative PCR. Relative expression of PIP5KIs normalized by cyclophilin B expression is shown. Data are mean ± SEM of three independent experiments. (b) MDA-MB-231 cells were transfected with non-silencing control (Ctrl), PIP5KIα, or Iγ siRNA, and subjected to RT-PCR (left) and immunoblot (right) analyses. Cyclophilin B (Cycl) and actin were used as controls. (c) Cells transfected with siRNAs were cultured on fluorescent gelatin-coated coverslips and stained with phalloidin to visualize invadopodia. (d) The degradation area of the gelatin was quantified among cells transfected with the indicated siRNAs. Data are mean ± SEM of four independent determinations. In each determination, at least 40 cells were analyzed. *$P < 0.02$ and ** $P < 0.0003$, Student's t-test.

Yamaguchi *et al.*

(Fig. 4a,b). The level of phospho-Akt in PIP5KIα knockdown cells was comparable to that in control cells (Fig. 4a,b). Total cellular content of PI(4,5)P$_2$ in PIP5KIα knockdown cells was also examined using an enzyme-linked immunosorbent assay (ELISA)-based method. This analysis showed that the total amount of PI(4,5)P$_2$ in PIP5KIα knockdown cells decreased to 61% of that in control cells (Fig. 4c). Because the PI(3,4,5)P$_3$ level is considerably lower than that of PI(4,5)P$_2$,[31] the reduction of PI(4,5)P$_2$ by PIP5KIα knockdown may have minimal effect on PI3K signaling.

PIP5KIα localizes at invadopodia. Localization of endogenous PIP5KIα at invadopodia was examined by immunocytochemistry. MDA-MB-231 cells were cultured on gelatin matrix and stained with anti-PIP5KIα antibody and phalloidin. PIP5KIα mainly localized at the plasma membrane (Fig. 5a). At the ventral membrane of the cells, the PIP5KIα signals accumulated at some invadopodia, but not all (Fig. 5a). To confirm the localization of PIP5KIα at invadopodia, cells were transfected with a GFP-PIP5KIα construct. The signals for GFP-PIP5KIα also accumulated at the gelatin degradation sites on the ventral cell membrane (Fig. 5b). These observations indicate that PIP5KIα localizes and functions at invadopodia.

Discussion

Here, we showed that PI(4,5)P$_2$ accumulates at invadopodia and that inhibition of PI(4,5)P$_2$ function by antibody microinjection or overexpression of PLCδ1-PH, a PI(4,5)P$_2$-binding domain, blocks invadopodia formation and ECM degradation by human breast cancer cells. Consistent with these results, a gelsolin peptide, which binds to and sequesters PI(4,5)P$_2$ in a similar manner to PLCδ1-PH, introduced into osteoclasts inhibits the formation of podosomes, structures closely related to invadopodia.[32] Moreover, Ziel et al.[33] recently reported that anchor cells form F-actin and PI(4,5)P$_2$-rich invasive protrusions of the ventral plasma membrane to invade the basement membrane in C. elegans. Although the functional relationship between these structures and invadopodia needs further investigation, PI(4,5)P$_2$ may have a conserved function in the formation of invasive membrane structures in a broad range of cell types.
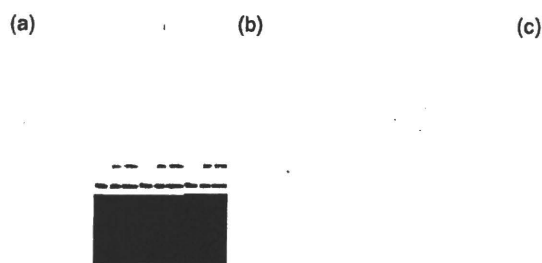
(a)   (b)   (c)

Fig. 4. PIP5KIα knockdown does not affect PI3K signaling. (a) MDA-MB-231 cells were transfected with non-silencing control (Ctrl) or PIP5KIα siRNA. The cells were serum-starved and stimulated with 50 ng/mL of EGF for 10 min. Cell lysates were then prepared and subjected to immunoblotting with antibodies against total and phospho-Akt. (b) The relative amount of phospho-Akt was calculated from the immunoblots. Data are mean ± SEM of four independent experiments. (c) Relative amount of cellular PI(4,5)P$_2$ was determined as described in the Materials and Methods. Data are mean ± SEM of four independent determinations. *$P < 0.002$, Student's t-test.
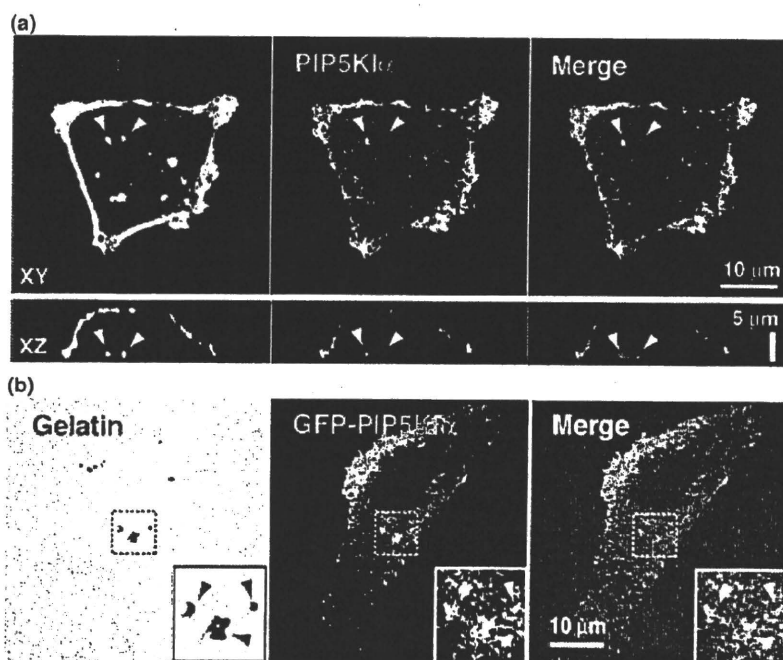

Fig. 5. PIP5KIα localizes at invadopodia. (a) MDA-MB-231 cells plated onto gelatin-coated coverslips were stained with anti-PIP5KIα antibody and phalloidin. Upper and lower images were XY and XZ sections obtained by confocal microscopy. Arrowheads denote invadopodia associated with PIP5KIα signals. (b) Cells transfected with the GFP-PIP5KIα construct were cultured on fluorescent gelatin and observed by confocal microscopy. Inserts are magnified images of the boxed regions. Arrowheads denote accumulation of GFP-PIP5KIα signals at the sites of gelatin degradation.

The staining of PI(4,5)P$_2$ were observed at vesicular structures surrounding invadopodia. These structures morphologically resemble the internalized lipid raft membranes that accumulate and traffic around invadopodia.[4] As disruption of lipid rafts inhibits invadopodia formation, these vesicular structures likely have an important role, such as trafficking of invadopodia components, in invadopodia biogenesis.[4] Previous studies have shown that PI(4,5)P$_2$ is enriched in lipid raft fractions, and promotes recruitment and activation of specific signaling components.[34] Therefore, PI(4,5)P$_2$ may regulate transport and activation of invadopodia components in these lipid raft-enriched vesicular structures.

PIP5KIs generate PI(4,5)P$_2$ and have been implicated in several cellular processes that require dynamic actin cytoskeleton, such as cell migration, endocytosis, phagocytosis, and neurite remodeling.[35] In this study, we found that PIP5KIα is an essential regulator of invadopodia formation and localizes at invadopodia; however, it is worth noting that PIP5KIα did not localize at all invadopodia. This observation suggests that PIP5KIα is not a structural component of invadopodia but rather has regulatory functions in invadopodia formation. It is possible that PIP5KIα is transiently recruited to invadopodia at specific stages of invadopodia formation.

Interestingly, PIP5KIα knockdown did not completely deplete cellular PI(4,5)P$_2$ and had little effect on the PI3K signaling pathway. This suggests that a pool of PI(4,5)P$_2$ locally produced by PIP5KIα directly regulates invadopodia formation rather than acting as a precursor for PI(3,4,5)P$_3$ formation. Because PI(4,5)P$_2$ directly binds to several components of invadopodia, such as N-WASP, cofilin, and dynamin-2,[19,20] it may control localization and/or activation of these proteins at invadopodia assembly sites.

Synaptojanin-2, which dephosphorylates PI(4,5)P$_2$ at the D-5 position on the inositol ring, localizes at invadopodia.[36] Given that PIP5KIα and synaptojanin-2 both localize and function at invadopodia, PI(4,5)P$_2$ turnover may play an important role in invadopodia formation. Supporting this idea, overexpression of

PIP5KIα in MDA-MB-231 cells, which should interfere with the PI(4,5)P$_2$ turnover, inhibited invadopodia formation (data not shown). In the endocytic process, local PI(4,5)P$_2$ turnover mediated by PIP5KI and synaptojanin is necessary for proper formation and internalization of clathrin-coated pits.[37] Therefore, it would be important to determine if similar PI(4,5)P$_2$ turnover occurs at invadopodia.

Arf6 is a small GTPase that has been implicated in the regulation of the actin cytoskeleton and membrane trafficking. These functions of Arf6 are at least partly mediated by the direct activation of PIP5KIs.[23,38] Recently, Arf6 has been reported to function in invadopodia-mediated cancer cell invasion.[21,22] Therefore, PIP5KIα may act as a downstream target of Arf6 for invadopodia formation. Further studies are needed to elucidate this possibility.

In conclusion, our results provide evidence that PI(4,5)P$_2$ and PIP5KIα are essential regulators of invadopodia formation. These findings identify a novel role for PI(4,5)P$_2$ in cancer cell invasion and should provide new insights into the molecular mechanisms of invadopodia formation. This will contribute to the development of new therapeutic strategies for cancer invasion and metastasis.

References

1 Buccione R, Caldieri G, Ayala I. Invadopodia: specialized tumor cell structures for the focal degradation of the extracellular matrix. *Cancer Metastasis Rev* 2009; **28**: 137–49.
2 Weaver AM. Invadopodia: specialized cell structures for cancer invasion. *Clin Exp Metastasis* 2006; **23**: 97–105.
3 Yamaguchi H, Lorenz M, Kempiak S *et al.* Molecular mechanisms of invadopodium formation: the role of the N-WASP-Arp2/3 complex pathway and cofilin. *J Cell Biol* 2005; **168**: 441–52.
4 Yamaguchi H, Takeo Y, Yoshida S, Kouchi Z, Nakamura Y, Fukami K. Lipid rafts and caveolin-1 are required for invadopodia formation and extracellular matrix degradation by human breast cancer cells. *Cancer Res* 2009; **69**: 8594–602.
5 Sidani M, Wyckoff J, Xue C, Segall JE, Condeelis J. Probing the microenvironment of mammary tumors using multiphoton microscopy. *J Mammary Gland Biol Neoplasia* 2006; **11**: 151–63.
6 Yamaguchi H, Wyckoff J, Condeelis J. Cell migration in tumors. *Curr Opin Cell Biol* 2005; **17**: 559–64.
7 Caldieri G, Buccione R. Aiming for invadopodia: organizing polarized delivery at sites of invasion. *Trends Cell Biol* 2010; **20**: 64–70.
8 Gimona M, Buccione R, Courtneidge SA, Linder S. Assembly and biological role of podosomes and invadopodia. *Curr Opin Cell Biol* 2008; **20**: 235–41.
9 Linder S. The matrix corroded: podosomes and invadopodia in extracellular matrix degradation. *Trends Cell Biol* 2007; **17**: 107–17.
10 Oser M, Yamaguchi H, Mader CC *et al.* Cortactin regulates cofilin and N-WASp activities to control the stages of invadopodium assembly and maturation. *J Cell Biol* 2009; **186**: 571–87.
11 Artym VV, Zhang Y, Seillier-Moiseiwitsch F, Yamada KM, Mueller SC. Dynamic interactions of cortactin and membrane type 1 matrix metalloproteinase at invadopodia: defining the stages of invadopodia formation and function. *Cancer Res* 2006; **66**: 3034–43.

12 Philippar U, Roussos ET, Oser M *et al.* A Mena invasion isoform potentiates EGF-induced carcinoma cell invasion and metastasis. *Dev Cell* 2008; **15**: 813–28.
13 Di Paolo G, DeCamilli P. Phosphoinositides in cell regulation and membrane dynamics. *Nature* 2006; **443**: 651–7.
14 Lemmon MA. Membrane recognition by phospholipid-binding domains. *Nat Rev Mol Cell Biol* 2008; **9**: 99–111.
15 Fruman DA, Meyers RE, Cantley LC. Phosphoinositide kinases. *Annu Rev Biochem* 1998; **67**: 481–507.
16 Anderson RA, Boronenkov IV, Doughman SD, Kunz J, Loijens JC. Phosphatidylinositol phosphate kinases, a multifaceted family of signaling enzymes. *J Biol Chem* 1999; **274**: 9907–10.
17 Balla A, Balla T. Phosphatidylinositol 4-kinases: old enzymes with emerging functions. *Trends Cell Biol* 2006; **16**: 351–61.
18 Doughman RL, Firestone AJ, Anderson RA. Phosphatidylinositol phosphate kinases put PI4,5P(2) in its place. *J Membr Biol* 2003; **194**: 77–89.
19 Ling K, Schill NJ, Wagoner MP, Sun Y, Anderson RA. Movin' on up: the role of PtdIns(4,5)P(2) in cell migration. *Trends Cell Biol* 2006; **16**: 276–84.
20 Takenawa T, Itoh T. Phosphoinositides, key molecules for regulation of actin cytoskeletal organization and membrane traffic from the plasma membrane. *Biochim Biophys Acta* 2001; **1533**: 190–206.
21 Hashimoto S, Onodera Y, Hashimoto A *et al.* Requirement for Arf6 in breast cancer invasive activities. *Proc Natl Acad Sci U S A* 2004; **101**: 6647–52.
22 Tague SE, Muralidharan V, D'Souza-Schorey C. ADP-ribosylation factor 6 regulates tumor cell invasion through the activation of the MEK/ERK signaling pathway. *Proc Natl Acad Sci U S A* 2004; **101**: 9671–6.
23 Funakoshi Y, Hasegawa H, Kanaho Y. Activation mechanisms of PIP5K isozymes by the small GTPase ARF6. *Adv Enzyme Regul.* 2009. doi:10.1016/j.advenzreg.2009.11.001.
24 Fukami K, Matsuoka K, Nakanishi O, Yamakawa A, Kawai S, Takenawa T. Antibody to phosphatidylinositol 4,5-bisphosphate inhibits oncogene-induced mitogenesis. *Proc Natl Acad Sci U S A* 1988; **85**: 9057–61.

Yamaguchi *et al.*

25 van Rheenen J, Song X, van Roosmalen W *et al.* EGF-induced PIP2 hydrolysis releases and activates cofilin locally in carcinoma cells. *J Cell Biol* 2007; 179: 1247–59.

26 Bowden ET, Coopman PJ, Mueller SC. Invadopodia: unique methods for measurement of extracellular matrix degradation in vitro. *Methods Cell Biol* 2001; 63: 613–27.

27 Neve RM, Chin K, Fridlyand J *et al.* A collection of breast cancer cell lines for the study of functionally distinct cancer subtypes. *Cancer Cell* 2006; 10: 515–27.

28 Balla T. Imaging and manipulating phosphoinositides in living cells. *J Physiol* 2007; 582: 927–37.

29 Yagisawa H, Sakuma K, Paterson HF *et al.* Replacements of single basic amino acids in the pleckstrin homology domain of phospholipase C-delta1 alter the ligand binding, phospholipase activity, and interaction with the plasma membrane. *J Biol Chem* 1998; 273: 417–24.

30 Nakahara H, Otani T, Sasaki T, Miura Y, Takai Y, Kogo M. Involvement of Cdc42 and Rac small G proteins in invadopodia formation of RPMI7951 cells. *Genes Cells* 2003; 8: 1019–27.

31 Pendaries C, Tronchere H, Plantavid M, Payrastre B. Phosphoinositide signaling disorders in human diseases. *FEBS Lett* 2003; 546: 25–31.

32 Biswas RS, Baker D, Hruska KA, Chellaiah MA. Polyphosphoinositides-dependent regulation of the osteoclast actin cytoskeleton and bone resorption. *BMC Cell Biol* 2004; 5: 19.

33 Ziel JW, Hagedorn EJ, Audhya A, Sherwood DR. UNC-6 (netrin) orients the invasive membrane of the anchor cell in C. elegans. *Nat Cell Biol* 2009; 11: 183–9.

34 Caroni P. Actin cytoskeleton regulation through modulation of PI(4,5)P$_2$ rafts. *EMBO J* 2001; 20: 4332–6.

35 Mao YS, Yin HL. Regulation of the actin cytoskeleton by phosphatidylinositol 4-phosphate 5 kinases. *Pflugers Arch* 2007; 455: 5–18.

36 Chuang YY, Tran NL, Rusk N, Nakada M, Berens ME, Symons M. Role of synaptojanin 2 in glioma cell migration and invasion. *Cancer Res* 2004; 64: 8271–5.

37 Sun Y, Carroll S, Kaksonen M, Toshima JY, Drubin DG. PtdIns(4,5)P2 turnover is required for multiple stages during clathrin- and actin-dependent endocytic internalization. *J Cell Biol* 2007; 177: 355–67.

38 Aikawa Y, Martin TF. ARF6 regulates a plasma membrane pool of phosphatidylinositol(4,5)bisphosphate required for regulated exocytosis. *J Cell Biol* 2003; 162: 647–59.

Cancer Research

AACR

CUB Domain–Containing Protein 1, a Prognostic Factor for Human Pancreatic Cancers, Promotes Cell Migration and Extracellular Matrix Degradation

Yuri Miyazawa, Takamasa Uekita, Nobuyoshi Hiraoka, et al.

Updated Version	Access the most recent version of this article at: doi:10.1158/0008-5472.CAN-10-0220
Supplementary Material	Access the most recent supplemental material at: http://cancerres.aacrjournals.org/content/suppl/2010/05/25/0008-5472.CAN-10-0220.DC1.html

Cited Articles	This article cites 30 articles, 14 of which you can access for free at: http://cancerres.aacrjournals.org/content/70/12/5136.full.html#ref-list-1
Citing Articles	This article has been cited by 2 HighWire-hosted articles. Access the articles at: http://cancerres.aacrjournals.org/content/70/12/5136.full.html#related-urls

E-mail alerts	Sign up to receive free email-alerts related to this article or journal.
Reprints and Subscriptions	To order reprints of this article or to subscribe to the journal, contact the AACR Publications Department at pubs@aacr.org.
Permissions	To request permission to re-use all or part of this article, contact the AACR Publications Department at permissions@aacr.org.

Tumor and Stem Cell Biology

Cancer Research

CUB Domain–Containing Protein 1, a Prognostic Factor for Human Pancreatic Cancers, Promotes Cell Migration and Extracellular Matrix Degradation

Yuri Miyazawa[1,4], Takamasa Uekita[1], Nobuyoshi Hiraoka[2], Satoko Fujii[1], Tomoo Kosuge[3], Yae Kanai[2], Yoshihisa Nojima[4], and Ryuichi Sakai[1]

Abstract

CUB domain–containing protein 1 (CDCP1) is a membrane protein that is highly expressed in several solid cancers. We reported previously that CDCP1 regulates anoikis resistance as well as cancer cell migration and invasion, although the underlying mechanisms have not been elucidated. In this study, we found that expression of CDCP1 in pancreatic cancer tissue was significantly correlated with overall survival and that CDCP1 expression in pancreatic cancer cell lines was relatively high among solid tumor cell lines. Reduction of CDCP1 expression in these cells suppressed extracellular matrix (ECM) degradation by inhibiting matrix metalloproteinase-9 secretion. Using the Y734F mutant of CDCP1, which lacks the tyrosine phosphorylation site, we showed that CDCP1 regulates cell migration, invasion, and ECM degradation in a tyrosine phosphorylation-dependent manner and that these CDCP1-associated characteristics were inhibited by blocking the association of CDCP1 and protein kinase Cδ (PKCδ). CDCP1 modulates the enzymatic activity of PKCδ through the tyrosine phosphorylation of PKCδ by recruiting PKCδ to Src family kinases. Cortactin, which was detected as a CDCP1-dependent binding partner of PKCδ, played a significant role in migration and invasion but not in ECM degradation of pancreatic cells. These results suggest that CDCP1 expression might play a crucial role in poor outcome of pancreatic cancer through promotion of invasion and metastasis and that molecules blocking the expression, phosphorylation, or the PKCδ-binding site of CDCP1 are potential therapeutic candidates. *Cancer Res; 70(12); 5136–46. ©2010 AACR.*

Introduction

CUB domain–containing protein 1 (CDCP1) is a type I transmembrane protein with several tyrosine residues that can be phosphorylated by Src family kinases (SFK; refs. 1–5). CDCP1 was first identified as the product of a gene preferentially expressed in colon cancer cells compared with normal tissue (1). We recently reported that tyrosine-phosphorylated CDCP1 in lung cancer cells plays a novel role in acquiring resistance to anoikis, a type of cell death caused by detachment from extracellular matrix (ECM). CDCP1 was reported to directly bind to protein kinase Cδ (PKCδ) at a unique C2 domain—a novel phosphotyrosine-binding domain—in a phosphorylation-dependent manner (4). The biological mean-

ing of interaction with PKCδ had not been revealed until we recently discovered that tyrosine-phosphorylated CDCP1 regulates the anoikis resistance of lung cancer cells by acting as a physical link between SFKs and PKCδ, which is a putative cell death–associated molecule (5). Using scirrhous gastric cancer cells, we further reported that phosphorylation of CDCP1 promotes cell migration and invasion *in vitro* and peritoneal dissemination *in vivo* in mice (6). Recent studies of lung adenocarcinoma and renal cell carcinoma have shown that CDCP1 expression has important associations with disease progression (7, 8). Despite accumulating evidence showing the significant involvement of CDCP1 in tumor progression, metastasis, and invasion, the role of the CDCP1 signaling pathway during these biological procedures is not yet well understood.

Pancreatic cancer is one of the most malignant tumors, with poor prognosis due to its aggressive behavior and high metastatic potential. Moreover, pancreatic cancer is sometimes accompanied with specific types of invasion, such as perineural invasion, which can cause severe pain and discomfort. Appropriate treatment that inhibits invasion and metastasis of pancreatic cancers is urgently required to improve both the survival and quality of life of patients.

In this study, we found that CDCP1 is expressed in primary pancreatic tumors as well as in sites of invasion and metastasis of pancreatic cancer. We analyzed the expression levels

Authors' Affiliations: ¹Growth Factor Division and ²Pathology Division, National Cancer Center Research Institute and ³Division of Hepato-Biliary and Pancreatic Surgery, National Cancer Center Hospital, Tokyo, Japan and ⁴Department of Medicine and Clinical Science, Gunma University Graduate School of Medicine, Gunma, Japan

American Association for Cancer Research

of CDCP1 protein in human pancreatic cancer tissues by using immunohistochemistry and discovered that high CDCP1 expression is correlated with poor prognosis. Tyrosine phosphorylation of CDCP1 was also shown to be essential for ECM degradation in pancreatic cancer through the formation of the CDCP1-PKCδ complex and enzymatic activation of PKCδ in highly invasive pancreatic cancer cell lines. Our results suggest that CDCP1 is a promising therapeutic target that modulates metastasis and invasion of several cancer types.

Materials and Methods

Cell culture and transfection

Pancreatic (Suit4, Capan1, PANC1, BxPC3, and CFPAC1) and gastric (HSC44As3 and HSC59) cancer cell lines were cultured in RPMI 1640 with 10% fetal bovine serum (FBS) at 37°C with 5% CO_2. The fibrosarcoma cell line HT1080 was cultured in DMEM with 10% FBS. For transfection, cells were seeded on a plate at 2.0×10^6 per 10-cm dish, and transfection was performed after 24 hours. Expression plasmids were transfected with Lipofectamine 2000 according to the manufacturer's instructions (Invitrogen). Transfected cells were selected in the presence of G418 at the concentration of 1,200 μg/mL (BxPC3) or 900 μg/mL (Capan1).

Short interfering RNA treatment

Two sets of short interfering RNAs (siRNA) of CDCP1 were synthesized as described elsewhere (5). Two sets of siRNAs of PKCδ or cortactin were synthesized as follows: PKCδ siRNA-1, 5′-GGUGCAGAAGAAGCCGACCAUGUAU-3′ (sense) and 5′-AUACAUGGUCGGCUUCUUCUGCACC-3′ (antisense); PKCδ siRNA-2, 5′-CCAAGGUGUUGAUGGUCGGUUCAGUA-3′ (sense) and 5′-UACUGAACCGACCAUCAACACCUUGG-3′ (antisense); cortactin siRNA-1, 5′-CCCAGAAAGACUAUGUGAAAGGGUU-3′ (sense) and 5′-AACCCUUUCACAUAGUCUUUCUGGG-3′ (antisense); cortactin siRNA-2, 5′-GGAGAAGCACGAGUCACAGAGAGAU-3′ (sense) and 5′-AUCUCUCUGUGACUCGUGCUUCUCC-3′ (antisense). The control siRNA was Stealth RNAi Negative Control Medium GC Duplex. All siRNAs were obtained from Invitrogen. siRNAs (40 pmol) were incorporated into cells using Lipofectamine 2000 according to the manufacturer's instructions. Cells were used for further experiments at 72 hours after siRNA treatment.

Plasmids, antibodies, and reagents

Plasmids of human CDCP1 and of CDCP1 Y734F (Tyr[734] to Phe) with FLAG tag have already been described (5). CDCP1 rescue mutant, which introduced silent mutations not to be suppressed by CDCP1 siRNA, with COOH terminus FLAG tag was generated by PCR using KOD-Plus-Mutagenesis kit (Toyobo Co. Ltd.). A cDNA fragment of the C2 domain of human PKCδ with hemagglutinin (HA) tag has already been described (5). The antibodies against PKCδ (C-20; 1:2,500), HA (Y-11; 1:2,500), and actin (I-19; 1:200) were purchased from Santa Cruz Biotechnology. The phospho-PKCδ (Tyr[311]; 1:500) and phospho-PKCδ (Thr[505]; 1:500) antibodies were

from Cell Signaling. The FLAG M2 (1:5,000) and α-tubulin (1:10,000) antibodies were from Sigma. Polyclonal antibody against CDCP1 (1:500) and tyrosine-phosphorylated CDCP1 (Tyr[734]; 1:1,000) was prepared as described previously (5). The monoclonal antibodies that recognize cortactin (clone 4F11; 1:5,000), matrix metalloproteinase-9 (MMP-9; 1:500), and phosphotyrosine (4G10; 1:2,500) were purchased from Millipore.

Western blotting and immunoprecipitation

Western blotting and immunoprecipitation were performed as described previously (5). Protein concentration was measured by bicinchoninic acid protein assay kit (Pierce). Supernatant was concentrated by 10% trichloroacetic acid precipitation, and then samples were washed twice with diethyl ether. Polyvinylidene difluoride membrane (Immobilon-P, Millipore) was used for the transfer membrane, and Blocking One (Nakarai Tesque) was used for the blocking of the membrane. For immunoprecipitation, 1,000 μg protein was mixed with 2 μg of each antibody, and then samples were rotated with protein G–Sepharose beads (GE Healthcare).

Cell migration and Matrigel invasion assay

Migration and invasion assay were performed using modified Transwell chambers with a polycarbonate nucleopore membrane (BD Falcon) as described previously (9). Cells treated with each siRNA were detached with trypsin-EDTA. Then, the cells in 100 μL of RPMI 1640 with 10% FBS were seeded onto the upper part of each chamber. After incubation for 6 hours for migration, and 18 hours (BxPC3) or 30 hours (Capan1) for invasion, the cells on the membrane were fixed. The totals of migrated or invaded cells were determined by counting the cells on the lower side of the membranes from two wells (two fields per membrane) at a magnification of ×100, and the extent of migration or invasion was expressed as the average ratio (number of cells transfected with siRNA per field/average number of cells transfected with control siRNA per field). The results were from three independent experiments.

ECM degradation assays

The 12-mm-round cover glasses were coated with fluorescein-conjugated type I collagen from bovine skin (Invitrogen) diluted at 1 μg/μL in PBS for 5 minutes at room temperature, and the cover glasses were dried out for 10 minutes at room temperature. The collagen-coated glasses were then fixed with 0.5% glutaraldehyde solution on ice for 10 minutes and at room temperature for 30 minutes. After washing six times with PBS, the glasses facing upward were transferred to each well of a 24-well plate containing 70% ethanol and incubated for 15 minutes. After two washes with PBS, 2×10^4 cells were plated onto the coated glass in RPMI 1640 containing 10% FBS. After 18 hours (BxPC3) or 30 hours (Capan1) of culture, cells were fixed and stained with Alexa phalloidin (1:100; Invitrogen) in PBS. The staining was visualized using a Radiance 2100 confocal microscopic system (Bio-Rad). The cells degrading collagen were determined to

overlap the degradation area. Data in 20 fields at a magnification of ×800 were used to calculate the cells degrading collagen per total cells. The results were from three independent experiments.

Gelatin zymography

Gelatin zymography was conducted with a polyacrylamide gel containing gelatin (0.8 mg/mL) as described previously (10). The SDS-polyacrylamide gel was incubated for 24 hours in the incubation buffer with or without 2.7 nmol/L MMP inhibitor II (MMP-1, MMP-3, MMP-7, and MMP-9 inhibitor; Calbiochem) or DMSO at 37°C. Enzyme activity was visualized as negative staining with Coomassie brilliant blue.

Immunocytochemical staining

Immunocytochemical staining was performed as previously described (11). The cover glasses were coated by FBS for 1 hour before seeding the cells. For transfection, 5.0×10^4 cells were seeded on a glass and then fixed and stained. The staining was visualized using a confocal microscopic system (Bio-Rad).

Patients and tissue samples

Pancreatic tumor specimens were obtained from 158 patients who underwent surgery at the National Cancer Center Hospital (1990–2005; clinicopathologic findings from these 158 patients are summarized in Supplementary Table S1). The follow-up period for survivors ranged from 0.067 to 172.833 months (median, 14.433 mo). Tumors were classified according to the International Union Against Cancer tumor-node-metastasis classification (12), the classification of pancreatic carcinoma of the Japan Pancreas Society (13), and the WHO classification (14). The study was approved by the ethical review board of the National Cancer Center. Informed consent was obtained from each patient.

Immunohistochemistry

Immunohistochemical staining was performed on the formalin-fixed, paraffin-embedded slides using the avidin-biotin complex method, as described previously (15). A specific antibody against CDCP1 (rabbit polyclonal antibody, 1:500) was used as the primary antibody. Staining in the absence of the primary antibody provided the negative control. The staining on each slide was evaluated by one researcher with two independent observations. Samples were blinded to clinicopathologic data and patient outcomes during observation. Immunoreactivity was scored semiquantitatively according to the estimated percentage of positive tumor cells (1, <50% reacting cells; 2, 50–80% reacting cells; 3, >80%) and intensity (1, weaker than the intensity of surface staining in the islet of Langerhans; 2, equal to the intensity of the islet of Langerhans; 3, stronger than the intensity of the islet of Langerhans). The slides, whose islet of Langerhans was not significantly stained, were considered to be in bad condition and were not evaluated. A total immunohistochemical score was calculated by summing the percentage score and the intensity score. The quantity of CDCP1 expression was classified into two groups by the total score (low group, 2–4; high group, 5 and 6).

Statistical analysis

We used the StatView software and SAS version 9.1.3 (SAS Institute, Inc.) for statistical analyses. Cochran-Armitage trend test and χ^2 test were used to assess the association between CDCP1 expression levels and clinicopathologic parameters (Supplementary Table S2). Kaplan-Meier methods were used to calculate overall survival, and differences in survival curves were evaluated with the log-rank test. The hazard ratios (HR) with 95% confidence intervals (CI) of the CDCP1 high-expression effect were estimated using univariate and multivariate Cox's proportional hazards model (Table 1). P values of <0.05 were considered to be statistically significant.

Results

CDCP1 expression is correlated with prognosis of patients with pancreatic cancer

During the screening for the protein expression of CDCP1 in various cancer cell lines, we noticed that CDCP1 is highly expressed and phosphorylated at tyrosines in most pancreatic cell lines (Fig. 1A). CDCP1 is also expressed in other cancer cells such as lung cancers and gastric cancers as we previously reported, whereas it is not expressed in some cancers such as neuroblastomas (data not shown). We further examined CDCP1 expression in human pancreatic cancer tissues by immunohistochemical analysis. Both well-differentiated and poorly differentiated types of pancreatic cancers were significantly stained with the CDCP1 antibody whereas normal pancreatic ducts were not obviously stained (Fig. 1B, a and b). CDCP1 staining was also detected in the perineural invasion site and at sites of lymph node metastasis (Fig. 1B, c–e). Expression levels of CDCP1 in poorly differentiated cancers are generally higher than in well-differentiated types, especially at invasion sites and metastatic loci. CDCP1 protein expression was examined in surgical specimens from 158 patients with pancreatic cancer. Expression levels of CDCP1 were evaluable in 145 cases, and they were classified into the low-expressing (63.4%, $n = 92$) and high-expressing (36.6%, $n = 53$) groups, as described in Materials and Methods. There were no significant associations in the clinicopathologic parameters between CDCP1 expression groups (Supplementary Table S2). The Kaplan-Meier plots also showed that there was a significant difference in overall survival rates ($P = 0.0391$) between groups with high and low CDCP1 expression (Fig. 1C). The effect of CDCP1 expression on overall survival is similar between univariate and multivariate analyses (Table 1).

Tyrosine-phosphorylated CDCP1 regulates cell migration and invasion

As pancreatic cancer cells with high metastatic potential, such as BxPC3 and CFPAC1, seemed to show relatively high phosphorylation levels of CDCP1 at tyrosines (Fig. 1A), we analyzed the role of phosphorylated CDCP1 in the invasion and metastasis of pancreatic cancers. Localization of CDCP1 was mainly detected at cell-cell contact in human tissue samples (Fig. 1B). CDCP1 was also expressed at cell-cell contact

Table 1. Univariate and multivariate analyses of prognostic factors for overall survival

	Overall survival			
	Univariate		Multivariate	
	HR (95% CI)	P	HR (95% CI)	P
Stage*	1.549 (1.275–1.883)	<0.0001	1.458 (1.185–1.795)	0.0004
Primary tumor*	2.833 (1.403–5.718)	0.0037	—	—
Regional lymph nodes*	2.963 (1.592–5.515)	0.0006	—	—
Distant metastasis*	1.994 (1.166–3.408)	0.0117	—	—
Histology[†‡]	1.340 (0.997–1.801)	0.0525		
Lymphatic invasion (ly0 + ly1 or ly2 + ly3)[†]	1.954 (1.381–2.765)	0.0002	1.507 (0.977–2.325)	0.0639
Venous invasion (v0 + v1 or v2 + v3)[†]	1.536 (1.093–2.160)	0.0136	1.308 (0.861–1.987)	0.2084
Intrapancreatic nerve invasion (n0 + n1 or n2 + n3)[†]	1.340 (0.953–1.884)	0.0923		
Spread within the main pancreatic duct [mpd (−) or mpd (b) + (+)][†]	1.065 (0.679–1.668)	0.7848		
CDCP1	1.470 (1.017–2.125)	0.0404	1.482 (1.022–2.150)	0.0381

Abbreviations: mpd, main pancreatic duct; b, borderline.
*Classified according to the classification of International Union Against Cancer.
[†]Classified according to the classification of pancreatic carcinoma of Japan Pancreas Society.
[‡]Classified according to the classification of WHO.

in pancreatic cancer cell lines, whereas much lower expression was detected at the free edges of cells (Supplementary Fig. S1).

Suppression of CDCP1 expression by siRNA strongly inhibited cell migration and invasion of pancreatic cancer cells (Fig. 2A; Supplementary Fig. S2). Similar to the previous report in lung cancer cells (5), downregulation of CDCP1 in pancreatic cancer cells had no significant effect on the phosphorylation of AKT and extracellular signal-regulated kinase 1/2, which are essential components of the growth factor signaling pathway mediating cell survival, proliferation, and motility (data not shown). For rescue experiments, vectors expressing wild-type CDCP1 and Y734F mutant CDCP1, which lacks the SFKs-binding site, were designed to contain silent mutations to be resistant to siRNA for CDCP1 as shown in Fig. 2B (CDCP1 res-F and Y734F res-F, respectively). Tyrosine phosphorylation of CDCP1 is shown to be attenuated in Y734F mutant through dissociation from SFKs (Supplementary Fig. S3). After suppression by CDCP1 siRNA, CDCP1 expression was restored by transfection of either CDCP1 res-F or Y734F res-F constructs in BxPC3 as expected (Fig. 2C). Both migration and invasion were recovered by the CDCP1 res-F construct to the level of original BxPC3 cells, but not by the Y734F res-F mutant (Fig. 2D), suggesting that CDCP1 regulates migration and invasion in a tyrosine phosphorylation–dependent manner.

Tyrosine-phosphorylated CDCP1 promotes ECM degradation

Because the biological role of CDCP1 in invasion is totally unknown, we first examined whether CDCP1 influences ECM degradation of cancer cells. Loss of CDCP1 decreased the ability to degrade fluorescence-conjugated collagen on cover glasses (Fig. 3A), whereas it caused no significant effect on

the degree of cell-ECM attachment (data not shown). To quantify the ability of ECM degradation, cells that are >50% covered by dark area with degraded collagen were counted, and the ratio to the total number of cells was calculated. This ratio of degradation showed 40% to 90% decrease in BxPC3 and Capan1 by suppression of CDCP1 (Fig. 3B). Protease secretion was then analyzed by zymography to identify factor (s) that regulates ECM degradation. Suppression of CDCP1 attenuated gelatin degradation bands at ~90 kDa detected in culture medium of BxPC3 and CFPAC1 (Fig. 3C, top; Supplementary Fig. S4). The bands at ~90 kDa in the zymogram correspond to the molecular size of MMP-9, a major MMP expressed in invasive cancer, and were actually detected by Western blotting using the anti–MMP-9 antibody (Fig. 3C, bottom left). Treatment of MMP inhibitor II, which inhibits a series of MMPs including MMP-9, suppressed the bands at ~90 kDa in both BxPC3 and HT1080, which is already known to secrete MMP-9 (Fig. 3C, bottom right), whereas the bands at ~60 kDa, presumably MMP-2, were not inhibited in HT1080 cells. The quantity of MMP-9 mRNA was not affected by CDCP1 siRNA (data not shown). These results indicate that CDCP1 controls ECM degradation through secretion of proteases, including MMP-9, in pancreatic cancer cells.

CDCP1 induces activation of PKCδ through tyrosine phosphorylation of PKCδ

It was shown in pancreatic cancer cell lines that tyrosine phosphorylation of CDCP1 at Tyr[734] triggers its association with a downstream target PKCδ, recruitment of PKCδ to the CDCP1-SFKs complex, and tyrosine phosphorylation of PKCδ (Fig. 2C; Supplementary Fig. S3), which is required for anoikis resistance of cancer cells (5). Suppression of PKCδ inhibited cell migration and invasion (Supplementary Fig. S5)

and also blocked ECM degradation and protease secretion in BxPC3 and CFPAC1 (Fig. 4A; data not shown). The overexpression of the HA-tagged C2 domain of PKCδ, which was designed to block the CDCP1-PKCδ interaction (4, 5), resulted in decrease of migration and invasion of Capan1 cells (Fig. 4B), suggesting the CDCP1-PKCδ association is essential for these characteristics. Moreover, the overexpression of Y734F-F mutant in BxPC3 decreased ECM degradation and the secretion of proteases, including MMP-9 (Fig. 4C). This Y734F-F mutant suppressed tyrosine phosphorylation of PKCδ without significantly affecting the phosphorylation states of wild-type CDCP1 (Fig. 4C), possibly by interfering the extracellular signal, which might also modulate CDCP1-PKCδ signal in a dominant-negative manner. Phosphorylation of PKCδ at Thr^{505}, which was reported to indicate kinase activity of PKCδ (16), was examined by using a phosphospe-

cific antibody. Phosphorylation of PKCδ at Thr^{505} was actually induced by treatment of phorbol 12-myristate 13-acetate (PMA), an activator of PKCs, whereas it was reduced by suppression of CDCP1 expression (Fig. 4D). It was indicated that tyrosine phosphorylation of PKCδ by CDCP1 affects the kinase activity of PKCδ.

Cortactin is a candidate protein downstream of the CDCP1-PKCδ pathway in cell migration and invasion

Treatment of CDCP1 siRNA did not cause significant effects on the phosphorylation status of several signaling proteins such as paxillin, focal adhesion kinase, and adducin, which were reported as downstream molecules of PKCδ (data not shown). On the other hand, we discovered that cortactin, which has been detected as one of the major substrates for SFKs and has been reported to play an essential
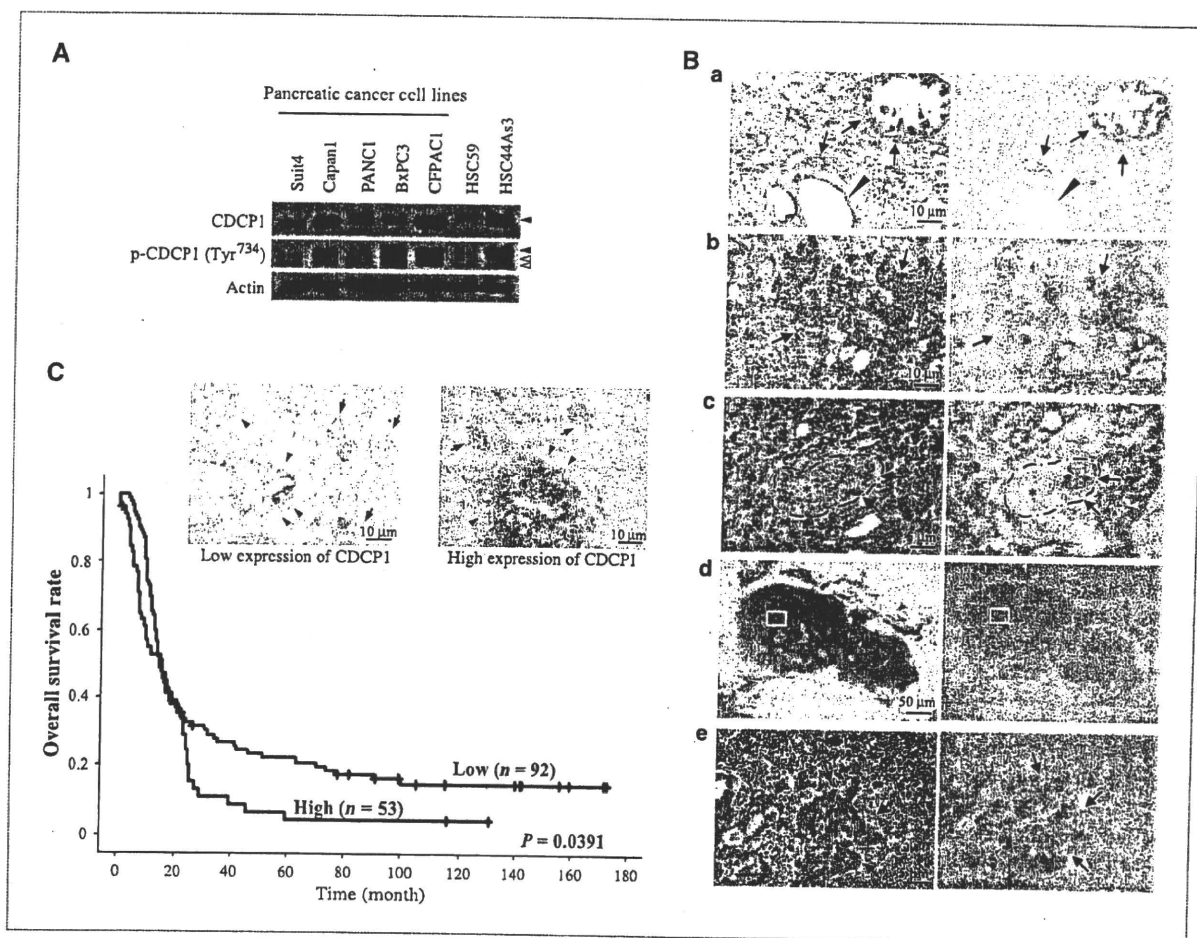

Figure 1. CDCP1 expression is correlated with prognosis of patients with pancreatic cancer. A, expression and tyrosine phosphorylation of CDCP1 in pancreatic cancer and noninvasive (HSC59) or invasive (HSC44As3) gastric cancer cell lines. Black arrowheads, CDCP1; white arrowheads, cross-reactive bands. B, CDCP1 expression in human pancreatic cancer tissues. Left, H&E staining; right, immunohistochemistry with anti-CDCP1 antibody. a, black arrowhead, normal pancreatic cells; black arrow, well-differentiated types of pancreatic cancers. b, poorly differentiated types of pancreatic cancers; c, perineural invasion (dotted line, epineurium; *, nerve); d and e, lymph node metastasis. e, enlargements of yellow squares in d. Magnifications, ×20 (d), ×100 (a and b), and ×200 (c and e). C, black arrowheads, pancreatic cancer; black arrows, islet of Langerhans for control staining. Kaplan-Meier plots of overall survival of patients with pancreatic cancer. High, CDCP1 high-expression group; Low, CDCP1 low-expression group.

Figure 2. CDCP1 regulates migration and invasion in a tyrosine phosphorylation–dependent manner. A, left, BxPC3 cells treated with CDCP1 siRNAs were used for immunoblotting with the indicated antibodies; right, migration and invasion assay of BxPC3 and Capan1 (4.0×10^4 cells) treated with CDCP1 siRNAs. Black arrowheads, CDCP1; white arrowheads, cross-reactive bands. B, schematic structure of CDCP1 and CDCP1 rescue mutant tagged with FLAG (CDCP1 res-F and Y734F res-F). The DNA base sequence that is not suppressed by CDCP1 siRNA is described. C, BxPC3 cells were treated with each siRNA and, 48 h later, transfected with the indicated plasmid. Cancer cells were used for immunoblotting with the indicated antibodies. Black arrowheads, CDCP1; white arrowheads, cross-reactive bands. D, migration and invasion assay using CDCP1 rescue mutant. BxPC3 cells treated with either control siRNA + pcDNA3.1 + pEGFP (bars, control + mock) or CDCP1 siRNA + each plasmid DNA + pEGFP (bars, mock, CDCP1 res-F, Y734F res-F) were used for each assay. Only migrated and invaded cells expressing green fluorescent protein (GFP) were counted using a fluorescence microscope. Columns, mean; bars, SD. The asterisks indicate statistically significant differences from the cells compared with control siRNA or control siRNA + Mock. *, $P < 0.05$; **, $P < 0.005$.
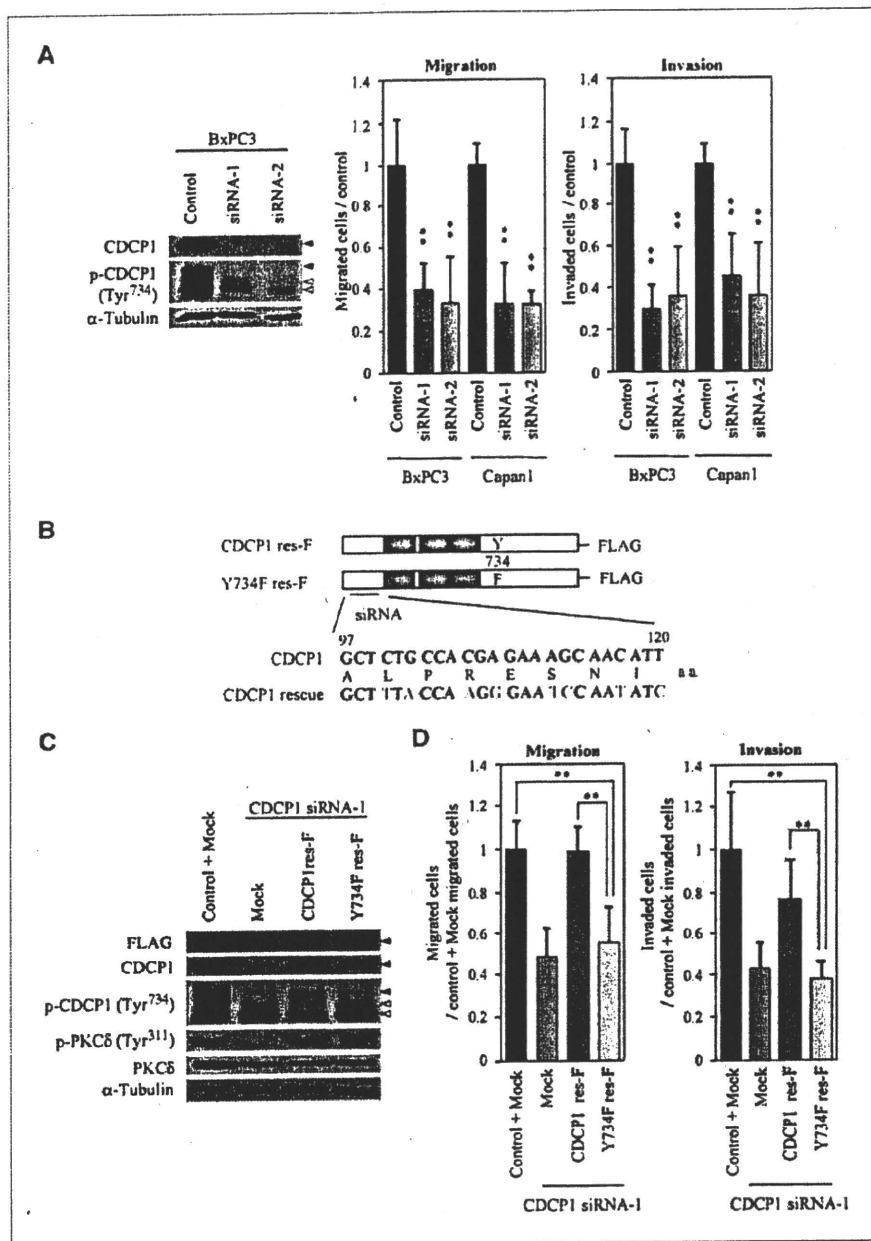
role in cell migration and invasion (17–19), was localized with CDCP1 and PKCδ at cell-cell contact in BxPC3 (Fig. 5A), and showed physical association with PKCδ through immunoprecipitation (Fig. 5B). Interestingly, suppression of CDCP1 disrupted the physical association between PKCδ and cortactin. On the other hand, tyrosine phosphorylation of cortactin was not affected by suppression of CDCP1 (Supplementary Fig. S6). Suppression of cortactin decreased migration and invasion in BxPC3 (Fig. 5C), as also reported in other cell types (20, 21), whereas it did not suppress ECM degradation (Fig. 5D) and gelatin degradation by proteases in the zymo-

gram (data not shown) in BxPC3 and CFPAC1 cells. These results suggest that cortactin might be one of the mediators of the CDCP1-PKCδ signaling complex in cancer cell migration but not in the ECM degradation.

Discussion

CDCP1 was originally identified as a membrane protein selectively expressed in the surface of metastatic cancers such as colon and lung cancers. It was later shown that CDCP1 is a potent substrate of SFKs *in vitro*, and our previous analysis

revealed that phosphorylation of CDCP1 by SFKs is essential for the anoikis resistance, which supports distant metastasis of solid cancers. In this study, we showed that CDCP1 is a significant prognostic factor that predicts the overall survival of patients with pancreatic cancer. We further showed for the first time that CDCP1-PKCδ signaling plays a crucial role in cell migration and ECM degradation in pancreatic cancer cells.

CDCP1 mRNA and protein expressions were found in various human solid cancers, including colon, lung, and breast cancers (1, 7, 22). CDCP1 was recently shown to be a prognostic factor of lung adenocarcinoma and renal cell carcinoma by using a large-scale analysis of CDCP1 expression in tumor samples (7, 8). By histologic analysis using human pancreatic cancer tissues, CDCP1 expression was detected not only in the original lesion but also in lymph node metastasis and perineural invasion (Fig. 1B). Pancreatic cancer is

one of the most frequent causes of cancer-related deaths worldwide. The poor prognosis is attributed to the high incidence of distant metastasis at the point of diagnosis and the highly invasive nature of this cancer. In that sense, it is important that the patients with high CDCP1 expression showed significantly worse overall survival on both univariate and multivariate analyses, suggesting that it might be a novel and independent prognostic factor of pancreatic cancer (Table 1). The individual clinicopathologic factors were not statistically significantly correlated with CDCP1 expression, which may be due to remarkably short overall survival in patients with pancreatic cancers compared with those with renal cell carcinomas or lung cancers. Although general prognostic markers such as p16, MMP-7, and vascular endothelial growth factor are also applicable to patients with pancreatic cancer (23), CDCP1 is an essential marker of poor
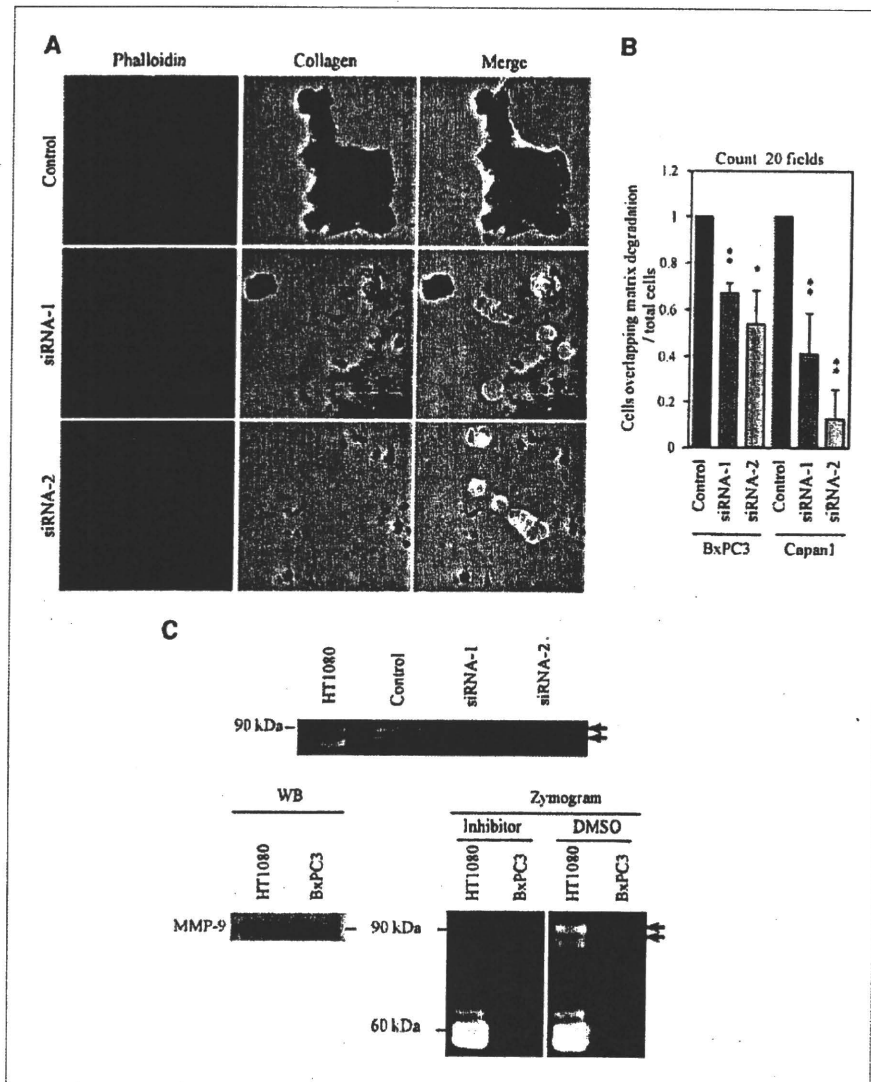

Figure 3. Tyrosine-phosphorylated CDCP1 promotes ECM degradation. A, BxPC3 cells transfected with CDCP1 siRNAs were incubated on covered glasses with fluorescein-conjugated collagen and stained with phalloidin to identify actin filaments. ECM degradation is identified as the dark area. B, quantification of ECM degradation. Cells overlapping the dark area, occupying more than half of the cell area, were counted. Columns, mean; bars, SD. The asterisks indicate statistically significant differences from the cells compared with control siRNA. *, $P < 0.05$; **, $P < 0.005$. C, top, gelatin zymography in BxPC3 transfected with CDCP1 siRNAs. Left, culture medium using BxPC3 and HT1080 cultures was concentrated and analyzed by Western blotting (WB) with the anti–MMP-9 antibody; right, zymogram of samples treated with MMP inhibitor II and DMSO. Black arrows, gelatin degradation.
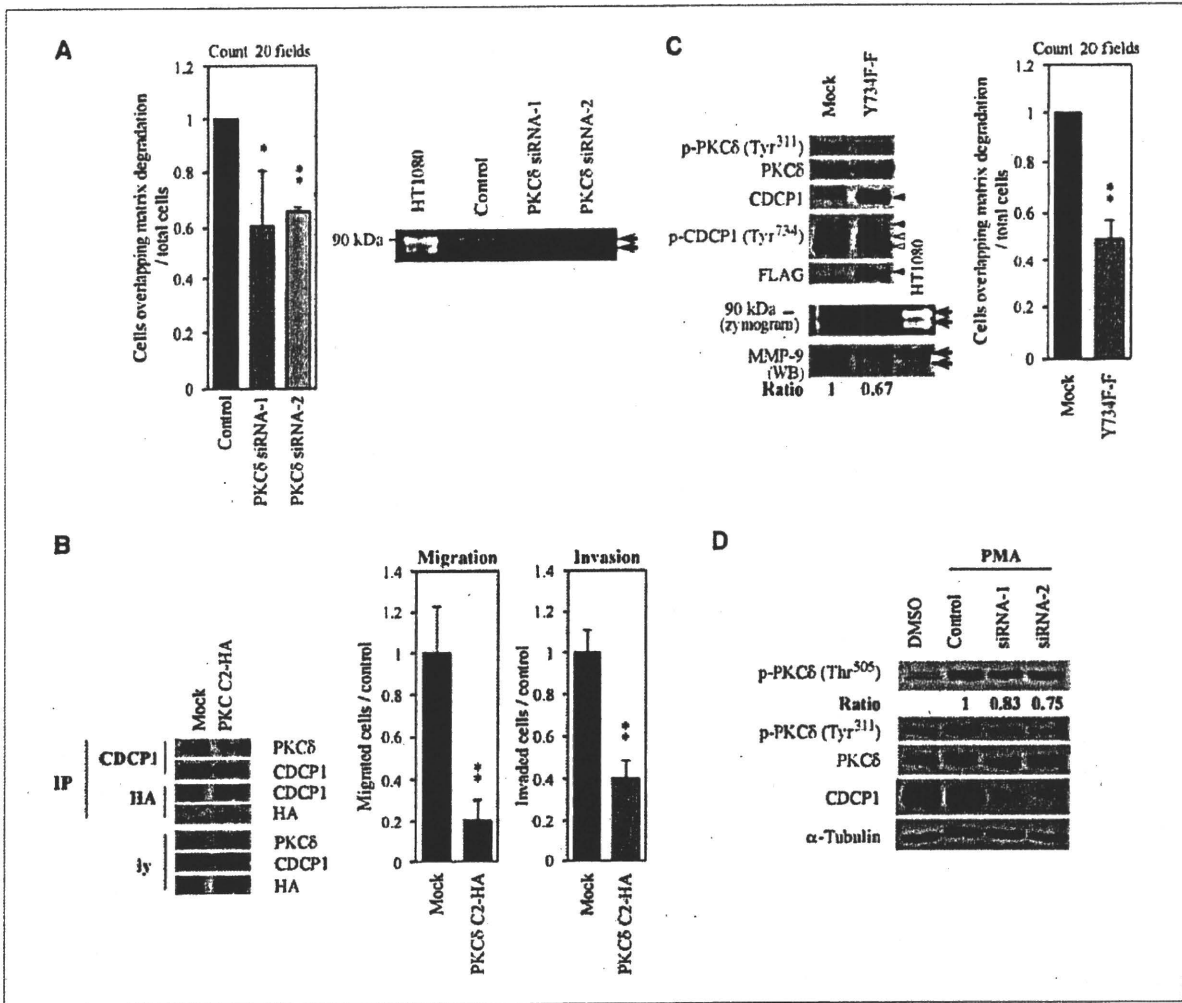
Figure 4. CDCP1 regulates migration and invasion via the PKCδ kinase activity. A, quantification of ECM degradation assay and zymogram of BxPC3 cells transfected with PKCδ siRNAs. Black arrows, MMP-9. B, left, Capan1 cells transfected with the C2 domain of PKCδ tagged with HA (PKCδ C2-HA) or pcDNA3.1 (Mock) were selected by G418. The lysate immunoprecipitated (IP) with anti-CDCP1 or anti-HA antibodies was used for immunoblotting with the indicated antibodies. Right, migration and invasion assay using Capan1 (4.0 × 10⁴ cells) transfected with the indicated plasmids. C, left, top, BxPC3 cells transfected with the CDCP1 mutant (Y734F res-F) or pcDNA3.1 (Mock) were selected by G418 and used for immunoblotting with the indicated antibodies; bottom, culture medium of the BxPC3 was analyzed by gelatin zymography and Western blotting with anti–MMP-9 antibody. Ratio, total MMP-9 of mock or Y734F/total MMP-9 of mock in Western blotting. Right, quantification of ECM degradation of BxPC3. Columns, mean; bars, SD. The asterisks indicate statistically significant differences from the cells transfected with control siRNA or mock. Black arrowheads, CDCP1; white arrowheads, cross-reactive bands; black arrows, MMP-9. *, $P < 0.05$; **, $P < 0.005$. D, BxPC3 cells transfected with CDCP1 siRNAs are cultured in 0.5% FBS for 24 h and treated with 100 nmol/L PMA or DMEM for 20 min at 37°C. The cells were used for immunoblotting with the indicated antibodies. Ratio, [phospho-PKCδ Thr⁵⁰⁵/PKCδ (each siRNA)]/[phspho-PKCδ Thr⁵⁰⁵/PKCδ (control siRNA)].

prognosis that is functionally related to particular malignant characteristics such as migration, ECM degradation, and anoikis resistance of cancer cells. This study also indicates that CDCP1 induces ECM degradation through secretion of proteases including MMP-9 (Figs. 3C and 4C). MMP-9 secretion has also been reported in human pancreatic tissue (24, 25) and was also considered to be a potential prognostic factor in pancreatic cancer (26).

A recent observation indicates that CDCP1 protein is expressed in some normal human tissues, such as the colon, breast, and lung, but not in the pancreatic duct (Fig. 1B), whereas the levels of CDCP1 phosphorylation in these normal tissues were much lower than those in cancer cells (27). We previously reported that phosphorylation of CDCP1 at Tyr⁷³⁴ is increased during peritoneal dissemination of gastric cancer in vivo and that it could promote migration of gastric cancer cells in vitro (6). In this study, we showed that phosphorylation of CDCP1 at Tyr⁷³⁴ plays a significant role in promotion of cell migration and ECM degradation, in addition to anoikis resistance of cancer cells. Therefore, it is

reasonable that not only the expression but also the tyrosine phosphorylation of CDCP1 is required for these characteristics of cancer cells associated with invasion and metastasis.

The complex formation between tyrosine-phosphorylated CDCP1 and PKCδ is required for the promotion of migration and ECM degradation. Our results also suggest that tyrosine phosphorylation of PKCδ, which was triggered by the association with phosphorylated CDCP1 coupled with SFKs, is essential for CDCP1-induced cell migration and ECM degradation. Judging from the levels of phosphorylation at Thr^{505} of PKCδ (Fig. 4D), a putative autophosphorylation site in an activation loop (16), tyrosine phosphorylation of PKCδ by the SFKs-CDCP1 pathway might activate PKCδ. Previous studies on PKCδ have shown that phosphorylation of PKCδ at Tyr^{311} results in enhanced phosphorylation at Thr^{505} (28) and that activation of PKCδ enhances the MMP-9 activity

(29). These findings suggest that the formation of the SFKs-CDCP1-PKCδ complex triggered by tyrosine phosphorylation of CDCP1 causes tyrosine phosphorylation of PKCδ and activation of kinase activity of PKCδ, which promotes cell migration and ECM degradation.

We identified cortactin as a binding partner of PKCδ. Cortactin is one of the key molecules that control cell migration and invasion. Some studies have reported that serine phosphorylation, but not tyrosine phosphorylation, of cortactin increases N-WASP binding and facilitates N-WASP–dependent actin polymerization (30, 31). Because the kinase activity of PKCδ (Fig. 4D) and the association of PKCδ and cortactin (Fig. 5B) can be affected by CDCP1, CDCP1 possibly regulates cell migration by altering serine/threonine phosphorylation of cortactin through PKCδ. Unfortunately, this could not be confirmed due to the lack of a good specific
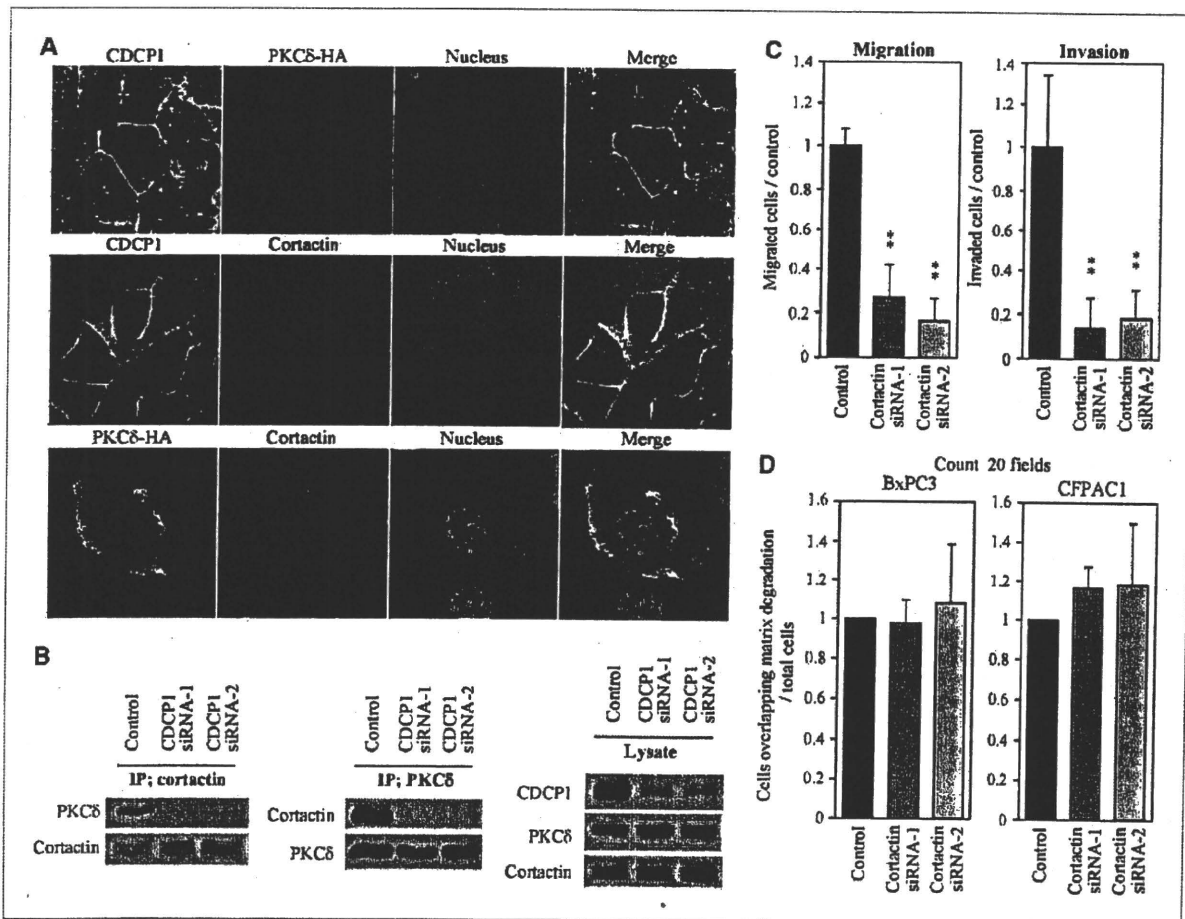

Figure 5. Cortactin, a PKCδ-associated protein, regulates cell migration and invasion. A, top, BxPC3 stained with anti-HA antibody (PKCδ-HA; red) and anti-CDCP1 antibody (green). The nucleus was stained with TOTO3. Middle, BxPC3 stained with anti-CDCP1 antibody (green) and anti-cortactin antibody (red). Bottom, BxPC3 stained with anti-HA antibody (PKCδ-HA; green) and anti-cortactin antibody (red). B, immunoprecipitation with anti-cortactin or anti-PKCδ antibodies in BxPC3 transfected with each siRNA. Samples were immunoblotted with the indicated antibodies. C, migration and invasion assay of BxPC3 (1.0×10^4 cells) transfected with cortactin siRNAs. Columns, mean; bars, SD. The asterisks indicate differences from cells treated with control siRNA. *, $P < 0.05$; **, $P < 0.005$. D, quantification of ECM degradation of protease in BxPC3.

antibody against serine/threonine–phosphorylated cortactin. Cortactin has also been reported to play a role in the function of invadopodia in several cancers (32, 33), although a structure similar to invadopodia was not found in the pancreatic cancer cells used in this study. Loss of cortactin did not suppress ECM degradation and protease secretion in pancreatic cancer cells, suggesting that some molecules other than cortactin might be regulating ECM degradation under the control of CDCP1, whereas cortactin is involved in CDCP1-induced migration of cells possibly through regulation of actin dynamics.

As CDCP1 binds the regulatory domain of SFKs (5), there is a possibility that CDCP1 controls the activity of SFKs by unfolding these proteins. Positive correlation between CDCP1 expression and Tyr[418] phosphorylation, which indicates autophosphorylation activity of SFKs, was obtained in BxPC3 cells (data not shown), whereas no clear correlation was obtained in other pancreatic cell lines. Further study will be required to understand the functional association between SFKs and CDCP1, including identification of other modulators of association.

Collectively, CDCP1 is a novel prognostic factor of pancreatic cancer, and inhibition of a specific cellular signal originating from the expression of phosphorylated CDCP1 has been shown to regulate cell migration, invasion, and ECM

degradation in pancreatic cancer cells. Because early clinical diagnosis of pancreatic cancer is difficult, invasion or metastasis to other organs frequently precedes diagnosis. In addition to its diagnostic usefulness as a membrane protein, CDCP1 might be an optimal therapeutic target of invasive and metastatic pancreatic cancers alone or combined with general chemotherapy drugs.

Disclosure of Potential Conflicts of Interest

Acknowledgments

Grant Support

References

1. Scherl-Mostageer M, Sommergruber W, Abseher R, Hauptmann R, Ambros P, Schweifer N. Identification of a novel gene, CDCP1, over-expressed in human colorectal cancer. Oncogene 2001;20:4402–8.

2. Hooper JD, Zijlstra A, Aimes RT, et al. Subtractive immunization using highly metastatic human tumor cells identifies SIMA135/CDCP1, a 135 kDa cell surface phosphorylated glycoprotein antigen. Oncogene 2003;22:1783–94.

3. Brown TA, Yang TM, Zaitsevskaia T, et al. Adhesion or plasmin regulates tyrosine phosphorylation of a novel membrane glycoprotein p80/gp140/CUB domain-containing protein 1 in epithelia. J Biol Chem 2004;279:14772–83.

4. Benes CH, Wu N, Elia AE, Dharia T, Cantley LC, Soltoff SP. The C2 domain of PKCδ is a phosphotyrosine binding domain. Cell 2005; 121:271–80.

5. Uekita T, Jia L, Narisawa-Saito M, Yokota J, Kiyono T, Sakai R. CUB domain-containing protein 1 is a novel regulator of anoikis resistance in lung adenocarcinoma. Mol Cell Biol 2007;27:7649–60.

6. Uekita T, Tanaka M, Takigahira M, et al. CUB-domain-containing protein 1 regulates peritoneal dissemination of gastric scirrhous carcinoma. Am J Pathol 2008;172:1729–39.

7. Ikeda J, Oda T, Inoue M, et al. Expression of CUB domain containing protein (CDCP1) is correlated with prognosis and survival of patients with adenocarcinoma of lung. Cancer Sci 2009;100:429–33.

8. Awakura Y, Nakamura E, Takahashi T, et al. Microarray-based identification of CUB-domain containing protein 1 as a potential prognostic marker in conventional renal cell carcinoma. J Cancer Res Clin Oncol 2008;134:1363–9.

9. Uekita T, Gotoh I, Kinoshita T, et al. Membrane-type 1 matrix metalloproteinase cytoplasmic tail-binding protein-1 is a new member of the Cupin superfamily. A possible multifunctional protein acting as an invasion suppressor down-regulated in tumors. J Biol Chem 2004; 279:12734–43.

10. Uekita T, Itoh Y, Yana I, Ohno H, Seiki M. Cytoplasmic tail-dependent internalization of membrane-type 1 matrix metalloproteinase is important for its invasion-promoting activity. J Cell Biol 2001; 155:1345–56.

11. Jia L, Uekita T, Sakai R. Hyperphosphorylated cortactin in cancer cells plays an inhibitory role in cell motility. Mol Cancer Res 2008; 6:654–62.

12. Sobin L, Wittekind C. TNM classification of malignant tumors. 6th ed. New York: Wiley-Liss; 2002. p. 93–6.

13. Japan Pancreatic Society. Classification of pancreatic carcinoma. 2nd English ed. Tokyo: Kanehara & Co.; 2003.

14. Klöppel G, Hruban RH, Longnecker DS, et al. Ductal adenocarcinoma of the pancreas. In: Hamilton SR, Aaltonen LA, editors. Pathology and genetics. Tumours of the digestive system. World Health Organization classification of tumours. Lyon (France): IARC Press; 2000, p. 221–30.

15. Takahashi Y, Hiraoka N, Onozato K, et al. Solid-pseudopapillary neoplasms of the pancreas in men and women: do they differ? Virchows Arch 2006;448:561–9.

16. Rybin VO, Sabri A, Short J, Braz JC, Molkentin JD, Steinberg SF. Cross-regulation of novel protein kinase C (PKC) isoform function in cardiomyocytes. Role of PKCε in activation loop phosphorylations and PKCδ in hydrophobic motif phosphorylations. J Biol Chem 2003; 278:14555–64.

17. Huang C, Liu J, Haudenschild CC, Zhan X. The role of tyrosine phosphorylation of cortactin in the locomotion of endothelial cells. J Biol Chem 1998;273:25770–6.

18. Huang J, Asawa T, Takato T, Sakai R. Cooperative roles of Fyn and cortactin in cell migration of metastatic murine melanoma. J Biol Chem 2003;278:48367–76.

19. Bryce NS, Clark ES, Leysath JL, Currie JD, Webb DJ, Weaver AM. Cortactin promotes cell motility by enhancing lamellipodial persistence. Curr Biol 2005;15:1276–85.

20. van Rossum AG, Moolenaar WH, Schuuring E. Cortactin affects cell migration by regulating intercellular adhesion and cell spreading. Exp Cell Res 2006;312:1658–70.

21. Yamaguchi H, Condeelis J. Regulation of the actin cytoskeleton in cancer cell migration and invasion. Biochim Biophys Acta 2007; 1773:642–52.

22. Bühring HJ, Kuçi S, Conze T, et al. CDCP1 identifies a broad

spectrum of normal and malignant stem/progenitor cell subsets of hematopoietic and nonhematopoietic origin. Stem Cells 2004;22: 334–43.

23. Tonini G, Pantano F, Vincenzi B, Gabbrielli A, Coppola R, Santini D. Molecular prognostic factors in patients with pancreatic cancer. Expert Opin Ther Targets 2007;11:1553–69.

24. Gress TM, Müller-Pillasch F, Lerch MM, Friess H, Büchler M, Adler G. Expression and in-situ localization of genes coding for extracellular matrix proteins and extracellular matrix degrading proteases in pancreatic cancer. Int J Cancer 1995;62:407–13.

25. Hirata M, Itoh M, Tsuchida A, Ooishi H, Hanada K, Kajiyama G. Cholecystokinin receptor antagonist, loxiglumide, inhibits invasiveness of human pancreatic cancer cell lines. FEBS Lett 1996;383:241–4.

26. Mroczko B, Lukaszewicz-Zajac M, Wereszczynska-Siemiatkowska U, et al. Clinical significance of the measurements of serum matrix metalloproteinase-9 and its inhibitor (tissue inhibitor of metalloproteinase-1) in patients with pancreatic cancer: metalloproteinase-9 as an independent prognostic factor. Pancreas 2009;38:613–8.

27. Wong CH, Baehner FL, Spassov DS, et al. Phosphorylation of the SRC epithelial substrate Trask is tightly regulated in normal epithelia but widespread in many human epithelial cancers. Clin Cancer Res 2009;15:2311–22.

28. Rybin VO, Guo J, Gertsberg Z, Elouardighi H, Steinberg SF. Protein kinase Cε (PKCε) and Src control PKCδ activation loop phosphorylation in cardiomyocytes. J Biol Chem 2007;282:23631–8.

29. Park SK, Hwang YS, Park KK, Park HJ, Seo JY, Chung WY. Kalopanax saponin A inhibits PMA-induced invasion by reducing matrix metalloproteinase-9 via PI3K/Akt- and PKCδ-mediated signaling in MCF-7 human breast cancer cells. Carcinogenesis 2009; 30:1225–33.

30. Campbell DH, Sutherland RL, Daly RJ. Signaling pathways and structural domains required for phosphorylation of EMS1/cortactin. Cancer Res 1999;59:5376–85.

31. Martinez-Quiles N, Ho HY, Kirschner MW, Ramesh N, Geha RS. Erk/ Src phosphorylation of cortactin acts as a switch on-switch off mechanism that controls its ability to activate N-WASP. Mol Cell Biol 2004;24:5269–80.

32. Bowden ET, Barth M, Thomas D, Glazer RI, Mueller SC. An invasion-related complex of cortactin, paxillin and PKCμ associates with invadopodia at sites of extracellular matrix degradation. Oncogene 1999; 18:4440–9.

33. Onodera Y, Hashimoto S, Hashimoto A, et al. Expression of AMAP1, an ArfGAP, provides novel targets to inhibit breast cancer invasive activities. EMBO J 2005;24:963–73.

p130Cas, Crk-Associated Substrate Plays Essential Roles in Liver Development by Regulating Sinusoidal Endothelial Cell Fenestration

Tatsuya Tazaki,[1]* Takaaki Sasaki,[1]* Kenta Uto,[3] Norimasa Yamasaki,[1] Satoshi Tashiro,[2] Ryuichi Sakai,[4] Minoru Tanaka,[5] Hideaki Oda,[3] Zen-Ichiro Honda,[6,7] and Hiroaki Honda[1]

p130Cas, Crk-associated substrate (Cas), is an adaptor/scaffold protein that plays a central role in actin cytoskeletal reorganization. We previously showed that mice in which Cas was deleted (Cas$^{-/-}$) died *in utero* because of early cardiovascular maldevelopment. To further investigate the *in vivo* roles of Cas, we generated mice with a hypomorphic Cas allele lacking the exon 2–derived region (Cas$^{\Delta ex2/\Delta ex2}$), which encodes Src homology domain 3 (SH3) of Cas. Cas$^{\Delta ex2/\Delta ex2}$ mice again died as embryos, but they particularly showed progressive liver degeneration with hepatocyte apoptosis. Because Cas expression in the liver is preferentially detected in sinusoidal endothelial cells (SECs), the observed hepatocyte apoptosis was most likely ascribable to impaired function of SECs. To address this possibility, we stably introduced a Cas mutant lacking the SH3 domain (Cas ΔSH3) into an SEC line (NP31). Intriguingly, the introduction of Cas ΔSH3 induced a loss of fenestrae, the characteristic cell-penetrating pores in SECs that serve as a critical route for supplying oxygen and nutrients to hepatocytes. The disappearance of fenestrae in Cas ΔSH3–expressing cells was associated with an attenuation of actin stress fiber formation, a marked reduction in tyrosine phosphorylation of Cas, and defective binding of Cas to CrkII. *Conclusion:* Cas plays pivotal roles in liver development through the reorganization of the actin cytoskeleton and formation of fenestrae in SECs. (HEPATOLOGY 2010;52:1089-1099)

The liver sinusoids are a unique multicellular system consisting of various cell types such as Kupffer cells, stellate cells, and sinusoidal endothelial cells (SECs).[1-3] These cells coordinately support and maintain hepatocyte survival, and their dysfunction results in hepatocyte apoptosis, which ultimately leads to liver failure.[2,4] SECs are not associated with basal laminas and possess characteristic cell-penetrating pores known as fenestrae.[1,3] Fenestrae provide a critical route for supplying oxygen and nutrients to hepatocytes and support the immunological contact of T cells with hepatocytes.[5,6] They are extremely sensitive to environmental conditions and change in number and diameter in response to external stimuli such as hormones, drugs, and toxins.[1,3] The molecular mechanisms regulating their structure are not fully understood, but previous studies have shown that the actin cytoskeleton is deeply involved.[1,3,7]

p130Cas, Crk-associated substrate (Cas), the gene product of breast cancer anti-estrogen resistance 1, was initially identified as an approximately 130-kDa, highly tyrosine-phosphorylated protein in cells transformed by v-src and v-crk oncoproteins.[8] It later became recognized as a central adaptor for actin cytoskeletal reorganization.[9,10] Under physiological conditions, Cas is phosphorylated on its tyrosines by stimuli that include integrin engagement, growth factor activation, mechanical stretching, and bacterial infection.[9,10] Cas is composed of several different protein-protein interaction domains: N-terminal Src homology domain 3 (SH3), a substrate domain (SD) containing multiple Tyr-x-x-Pro (YxxP) motifs, and a C-terminal Src-binding domain (SBD).[8,10] The SH3 domain binds to signaling molecules via their proline-rich domains, which include focal adhesion kinase,[11] focal adhesion kinase–related nonkinase,[12] proline-rich tyrosine kinase 2,[13] protein tyrosine phosphatase 1B,[14] protein tyrosine phosphatase–PEST (proline, glutamate, serine, and threonine),[15] guanine nucleotide exchange factor C3G,[16] and zinc finger protein CIZ (Cas-interacting zinc finger protein).[17] The multiple YxxP motifs in the SD serve as docking sites for the Src homology domain 2 (SH2) domains of the adaptor proteins CrkII[18] and non catalytic region of tyrosine kinase adaptor protein (Nck)[19] and for the SH2 domain containing inositol 5-phosphatase 2.[20] The SB domain contains a proline-rich motif and a YxxP motif, which bind to the SH3 and SH2 regions of Src, respectively.[21] Thus, Cas has a modular structure, and the individual module transmits signals by interacting with selected intracellular molecules.

We previously reported that Cas-deficient (Cas$^{-/-}$) mice died in utero at 12.5 days post coitum (dpc) and showed retarded cardiac development with disorganized myofibrils and disrupted Z-disks.[22] We also observed that Cas$^{-/-}$ fibroblasts had impaired actin stress fiber formation and profound defects in cell motility, migration, and spreading.[22,23] These results demonstrated that Cas functions as an actin-assembling molecule and plays vital roles in cell dynamics and organ development. To further understand the roles of Cas in organogenesis, we generated mice with a hypomorphic Cas allele devoid of the exon 2–derived region (Cas$^{\Delta ex2/\Delta ex2}$) encoding the entire SH3 domain. Interestingly, although Cas$^{\Delta ex2/\Delta ex2}$ mice also died as embryos, they had no cardiovascular system defects but instead showed progressive liver degeneration with hepatocyte apoptosis. Because Cas expression in the liver was not found in hepatocytes but was detected in SECs, it is likely that exon 2–deleted Cas (Cas Δex2) indirectly affects hepatocyte survival by altering SEC function. By employing an SEC line as an in vitro model system, we demonstrated that Cas lacking SH3, which possesses biochemical properties similar to those of Cas Δex2, resulted in impaired actin stress fiber formation and loss of fenestrae in SECs. These results indicated that Cas plays pivotal roles in liver development through the regulation of SEC fenestration.

Materials and Methods

Construction of the Targeting Vector and Generation of Cas$^{\Delta ex2/\Delta ex2}$ Mice. The construction of the targeting vector and the generation of Cas$^{\Delta ex2/\Delta ex2}$ mice are described in detail in the supporting information.

Western Blotting and Immunoprecipitation. Western blotting and immunoprecipitation were performed as described.[22] The procedure and antibodies used for the experiments are described in detail in the supporting information.

Histological, Immunohistochemical, Immunocytochemical, and Immunofluorescent Analyses. Histological, immunohistochemical, immunocytochemical, and immunofluorescent analyses were performed as described.[22] The procedure and antibodies used for the experiments are described in detail in the supporting information.

Terminal Deoxynucleotidyl Transferase–Mediated Deoxyuridine Triphosphate Nick-End Labeling (TUNEL) Assay. The TUNEL assay was performed with the ApopTag peroxidase in situ oligo ligation detection kit (Chemicon, Temecula, CA) according to the manufacturer's instructions.

Separation of Hepatic Parenchymal and Nonparenchymal Cells. The separation of hepatic parenchymal

and nonparenchymal cells was performed essentially as previously described.[24] The procedure is described in detail in the supporting information.

Culture of NP31 SECs. A rat hepatic SEC line (NP31)[25] was cultured on type I collagen–coated dishes (Iwaki, Chiba, Japan) in Dulbecco's modified Eagle's medium with 10% fetal bovine serum, penicillin (100 U/mL), and streptomycin (100 μg/mL) at 37°C with 5% CO_2.

Retrovirus Infection. A retrovirus vector (pMxIG)[26] and a retrovirus packaging cell line (Plat-E)[27] were used to generate recombinant retroviruses. Hemagglutinin (HA)-tagged complementary DNAs (cDNAs) of full-length Cas (Cas FL) and a Cas mutant lacking the SH3 domain (Cas ΔSH3)[28] were subcloned into pMxIG, and ecotropic retroviruses were produced by the transient transfection of Plat-E cells with viral vectors using FuGENE (Roche, Basel, Switzerland). Infection was performed in the presence of 8 μg/mL Polybrene (Sigma, St Louis, MO).

Cytoskeletal Staining. After fixation in 4% paraformaldehyde in phosphate-buffered saline for 10 minutes, cells were permeabilized with 0.5% Triton X-100 in phosphate-buffered saline for 5 minutes at room temperature and incubated with Alexa 594–conjugated phalloidin (1:40; Invitrogen, Carlsbad, CA) in 1% bovine serum albumin in phosphate-buffered saline for 30 minutes at 37°C. Cells were mounted with Vectashield and observed on an Axioplan2 microscope with AxioCam MRm controlled by Axiovision software (Carl Zeiss, Germany).

Electron Microscopy. NP31 cells, cultured on glass cover slips, were fixed in 2% glutaraldehyde buffered with a 1 M cacodylate buffer (pH 7.4) for 12 hours at 4°C and then with 1% osmium tetroxide in a cacodylate buffer (pH 7.4) for 1 hour at 4°C. After dehydration in a graded series of ethanol solutions, cells were dried to a critical point and sputter-coated with osmium. Cell surfaces were examined with an S-4300 scanning microscope (Hitachi, Tokyo, Japan) at a 30-kV accelerating voltage.

Results

Generation of Mice Deficient in Cas Exon 2. To create a reduction-of-function Cas allele by gene targeting, we deleted exon 2 of the Cas gene, which encodes the entire SH3 and the N-terminal part of the SD domain containing one YLVP motif and four YQxP motifs. To this end, we constructed a targeting vector containing Cas exon 2 flanked by two locus of X-over P1 (*loxP*) sequences and followed by the *Frt*-

flanked neomycin resistance (*Neo*) gene (Fig. 1A). When the floxed Cas exon 2 was correctly excised, exon 1 joined in frame to exon 3, and this resulted in a Cas transcript devoid of the exon 2–derived segment. Correctly targeted embryonic stem cells, identified by Southern blotting and genomic polymerase chain reaction (PCR; Fig. 1B, left and middle panels), were selected and used for the generation of heterozygous mice (Cas$^{+/floxNeo}$). The *Frt*-flanked *Neo* gene and floxed Cas exon 2 were sequentially deleted with flippase recombinase e (Flpe) and cyclization recombination (Cre) recombinases to generate *flox* and $\Delta ex2$ alleles, respectively. The genomic deletions were confirmed by internal genomic PCR (Fig. 1B, right panel). The structure of the resultant protein encoded by the $\Delta ex2$ allele (Cas $\Delta ex2$) is shown at the bottom of Fig. 1A. As shown by western blotting (Fig. 1C), a protein of the expected molecular weight (~90 kDa) was detected in the sample from Cas$^{\Delta ex2/\Delta ex2}$ mice (Cas $\Delta ex2$), and this indicated correct targeting, the excision of Cas exon 2, and the production of the short Cas protein lacking the corresponding segment.

Mice Deficient in Cas Exon 2 Died In Utero and Showed Impaired Liver Development with Progressive Hepatocyte Reduction Due to Apoptosis. Heterozygous (Cas$^{+/\Delta ex2}$) mice were apparently normal and were intercrossed to produce homozygous (Cas$^{\Delta ex2/\Delta ex2}$) mutants. No live Cas$^{\Delta ex2/\Delta ex2}$ neonates were obtained, and this indicated that the Cas$^{\Delta ex2/\Delta ex2}$ mice died as embryos. To investigate the date of embryonic lethality, embryos obtained from the intercrossing of Cas$^{+/\Delta ex2}$ mice were examined at different embryonic stages. As shown in Table 1, Cas$^{\Delta ex2/\Delta ex2}$ embryos were alive until 12.5 dpc, but no live Cas$^{\Delta ex2/\Delta ex2}$ embryos were obtained after 13.5 dpc.

To examine the cause of embryonic lethality in Cas$^{\Delta ex2/\Delta ex2}$ mice, wild-type (WT) and Cas$^{\Delta ex2/\Delta ex2}$ embryos at approximately 12.5 dpc were subjected to pathological examination. A remarkable and progressive change was observed in the livers of Cas$^{\Delta ex2/\Delta ex2}$ embryos. At 11.5 dpc, when macroscopic change was not yet apparent (Fig. 2A, left panels), hematoxylin and eosin (HE)–stained sections revealed that part of the liver of a Cas$^{\Delta ex2/\Delta ex2}$ embryo began to collapse from the inside (Fig. 2B, second bottom panel). At 12.5 dpc, this change was more pronounced, and the liver capsule of a Cas$^{\Delta ex2/\Delta ex2}$ embryo was macroscopically enlarged with a mass left inside (Fig. 2A, fourth panel). HE-stained sections showed that most of the hepatocytes were lost, whereas hematopoietic cells were preserved (Fig. 2B, fourth bottom panel). Despite intensive analysis, no pathological abnormalities were